Journal of Luminescence 132 (2012) 2439–2442

Contents lists available at SciVerse ScienceDirect

Journal of Luminescence

journal homepage: www.elsevier.com/locate/jlumin

Spectral tuning and energy transfer in a potential fluorescent lamp phosphor $BaMg_2Al_6Si_9O_{30}:Eu^{2+}$

Wei Lü [a,b], Yongshi Luo [a,*], Zhendong Hao [a], Xia Zhang [a], Xiaojun Wang [c], Jiahua Zhang [a,**]

[a] *Key Laboratory of Excited State Processes, Changchun Institute of Optics, Fine Mechanics and Physics, Chinese Academy of Sciences, Changchun 130033, China*
[b] *Graduate School of Chinese Academy of Sciences, Beijing 100039, China*
[c] *Department of Physics, Georgia Southern University, Statesboro, GA 30460, USA*

ARTICLE INFO

Article history:
Received 21 November 2011
Received in revised form
6 April 2012
Accepted 16 April 2012
Available online 25 April 2012

Keywords:
Phosphor
Energy transfer
Fluorescent lamp

ABSTRACT

$BaMg_2Al_6Si_9O_{30}:Eu^{2+}$ phosphors are synthesized by the solid-state reaction method and their photoluminescence (PL) properties are investigated. The ultraviolet emission originates from Eu^{2+}(I) substituting for Ba^{2+} sites, whereas the blue emission is attributed to Eu^{2+}(II) substituting for Mg^{2+} sites. With increasing Eu^{2+} doping concentrations, the blue emission band shifts to long wavelength and the PL intensity ratio of blue to ultraviolet emission increases. Energy transfer between the two different Eu^{2+} ions is analyzed by photoluminescence excitation and emission spectra, and lifetimes. Results indicate that the emission spectra can be tuned by changing Eu^{2+} contents. We have also demonstrated that $BaMg_2Al_6Si_9O_{30}:Eu^{2+}$ phosphor is a kind of potential phosphor for fluorescent lamps.

1. Introduction

Fluorescent lamps (FLs), after a half century of their practical use, are still the major light sources because of their high efficiency and long life. Although the basics of commercial triphosphors—the blue-emitting $BaMgAl_{10}O_{17}:Eu^{2+}$ [1], the red-emitting $Y_2O_3:Eu^{3+}$ [2], and the green-emitting $LaPO_4:Ce^{3+}, Tb^{3+}$ [3] were well established, the development of new phosphors continues because of the importance of phosphor efficiency required for different applications as well as for the production cost. In recent years, researchers have extensively investigated various rare-earth ions doped luminescent materials for the excitation wavelength of 254 nm [4–8]. However, single-phased full-color emitting phosphors for FL application were rarely reported.

In our previous work, we synthesized a series of $BaMg_2Al_6Si_9O_{30}:Eu^{2+}$, Tb^{3+}, and Mn^{2+} phosphors suitable for UV excitations [9]. But we had never systematically investigated the Eu^{2+} contents effect on the emission spectra of $BaMg_2Al_6Si_9O_{30}:Eu^{2+}$. In this work, not only the luminescence properties but also the energy transfers in $BaMg_2Al_6Si_9O_{30}:Eu^{2+}$ with various Eu^{2+} concentrations, are studied. These results demonstrate that the emission spectra can be tuned with changing concentrations of Eu^{2+} ions. By using the optimized Eu^{2+} content, white light emitting BMAS:Eu^{2+}, Tb^{3+}, and Mn^{2+} phosphors can be generated with higher color stability upon 254 nm excitation.

2. Experimental

The $Ba_{1-x}Mg_2Al_6Si_9O_{30}$ (BMAS):xEu^{2+} phosphors were synthesized by a high-temperature solid-state reaction. The constituent oxides or carbonates $BaCO_3$ (99.9%), Al_2O_3 (99.9%), SiO_2 (99.9%), MgO(99.9%), Eu_2O_3 (99.99%), and $MnCO_3$ (99.99%) were employed as the raw materials, which were mixed homogeneously by an agate mortar and pestled for 30 min, placed in a crucible with a lid, and then sintered in a tubular furnace at 1300 °C for 4 h in reductive atmosphere (10% H_2+90% N_2 mixed flowing gas).

Powder X-ray diffraction (XRD) data were collected using Cu Kα radiation (λ=1.54056 Å) on a Bruker D8 Advance diffractometer equipped with a linear position-sensitive detector (PSD-50m, M. Braun), operating at 40 kV and 40 mA with a step size of 0.02° (2θ) in the range 10–70°. The measurements of photoluminescence (PL) and photoluminescence excitation (PLE) spectra were performed by using a Hitachi F4500 spectrometer equipped with a 150 W xenon lamp under a working voltage of 700 V. The excitation and emission slits were both set at 2.5 nm. In fluorescence lifetime measurements, the third harmonic (266 nm) of an Nd-doped yttrium aluminum garnet pulsed laser (Spectra–Physics, GCR 130) was used as the excitation source, and the signals were detected with a Tektronix digital oscilloscope (TDS 3052).

---

[*] Corresponding author.
[**] Corresponding author. Tel./fax: +86 43 186176317.
E-mail address: zhangjh@ciomp.ac.cn (J. Zhang).

0022-2313/$ - see front matter © 2012 Elsevier B.V. All rights reserved.
http://dx.doi.org/10.1016/j.jlumin.2012.04.016

3. Result and discussion

Fig. 1 shows the XRD patterns of BMAS:Eu^{2+} with various Eu^{2+} concentrations. The XRD patterns of all phosphors are similar to JCPDS 83-0740 [10] of the BMAS host structure. Results indicate that doped Eu^{2+} ions do not cause any significant change in the host structure.

Fig. 2(a) shows the PL spectra ($\lambda_{ex}=330$ nm) of Eu^{2+}-activated BMAS as a function of Eu^{2+} concentration ranging from 0.005 to 0.1 mol. The PL spectra of BMAS consist of two distinct bands located at 376 and 450 nm under the excitation wavelength of 330 nm. The band emission is due to the $4f^65d^1 \rightarrow 4f^7$ transition of Eu^{2+} ion. As discussed in our previous work [9,11], $BaMg_2Al_6Si_9O_{30}$ crystallizes into a hexagonal structure with space group P6/mcc and has two types of independent cation sites, 12-fold coordinated Ba^{2+} site and 6-fold coordinated Mg^{2+} site. The PL spectra of Eu^{2+} in BMAS exhibit two PL bands, indicating the two cation sites. The average interatomic length between Eu^{2+} and oxygen (d_{Eu-O}) is 3.111 Å for Eu^{2+} occupying the Ba^{2+} site and 2.138 Å for occupying the Mg^{2+}site. Therefore we speculate that the band at 376 nm is assigned to Eu^{2+}(I) occupying Ba^{2+} with weak crystal field, and the other one at 450 nm corresponds to Eu^{2+}(II) occupying Mg^{2+} with strong crystal field. By changing the x value from 0.005 to 0.1, the PL intensity ratio of blue (I_B) to ultraviolet (I_U) emission increases. As shown in Fig. 2(b), this phenomenon can be explained by the energy transfer from Eu^{2+}(I) to Eu^{2+}(II). As we know, the distance between Eu^{2+} ions is reduced with increasing Eu^{2+} contents, and then the energy transfer from Eu^{2+}(I) to Eu^{2+}(II) happens. Fig. 3 presents the emission and excitation spectra of BMAS:Eu^{2+}. The shape of the PLE spectrum monitored at 376 nm (a) is remarkably different from that monitored at 450 nm (b). It further confirms that the two emission bands are originated from the Eu^{2+} ions occupying two different cation sites. Obviously, there is a significant spectral overlap between the Eu^{2+}(I) PL and Eu^{2+}(II) PLE spectra in the range 350–420 nm, which implies the possibility of energy transfer from Eu^{2+}(I) to Eu^{2+}(II). The energy transfer between two different Eu^{2+} ions would result in the enhancement of the blue (I_B) relative to ultraviolet (I_U) band in these phases. In addition, the Eu^{2+}(II) emission bands shift to long wavelength by about 26 nm with increasing Eu^{2+} concentrations, as presented in Fig. 2. The redshift can be ascribed to the energy transfer among Eu^{2+}(II) ions. In fact, as Eu^{2+} concentrations increase, the distance among Eu^{2+}(II) ions becomes shorter, which consequently increases the probability of energy transfer among

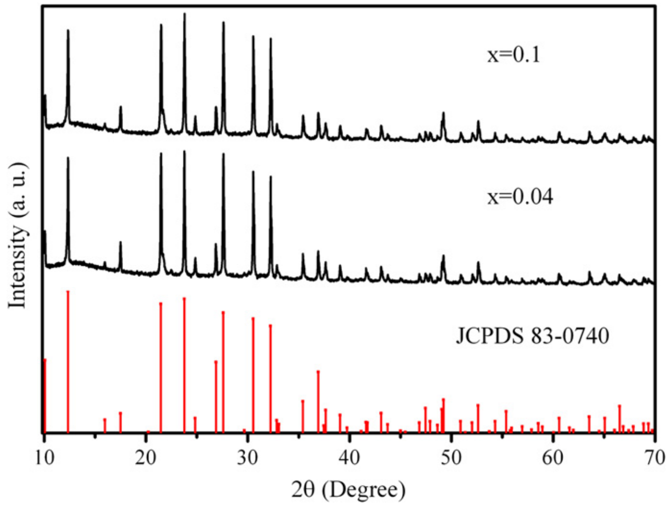

Fig. 1. XRD patterns of BMAS:Eu^{2+} with various Eu^{2+} concentrations.

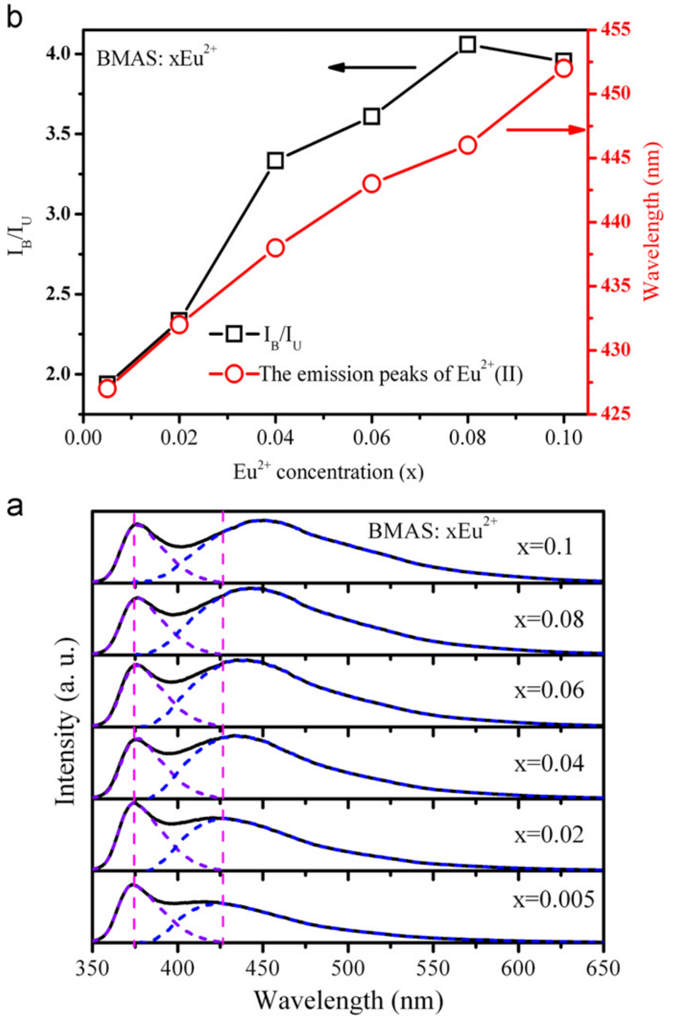

Fig. 2. (a) PL spectra of the Eu^{2+}-activated BMAS as a function of Eu^{2+} concentration ranging from 0.005 to 0.1 mol ($\lambda_{ex}=330$ nm) and (b) concentration dependence of the PL intensity ratio of blue (I_B) to ultraviolet (I_U) emission and the emission peaks of Eu^{2+}(II).

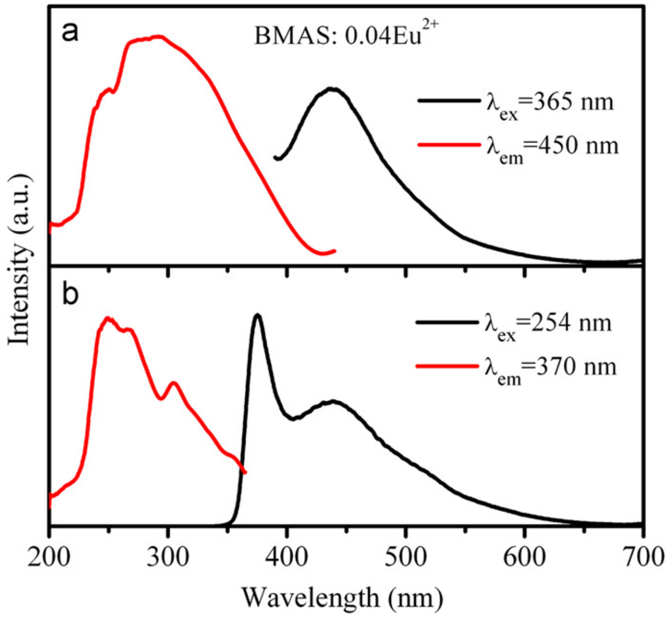

Fig. 3. Emission and excitation spectra of BMAS:Eu^{2+} sample.

Eu^{2+}(II) ions. This causes the emission energy of Eu^{2+} ions from the higher 5d levels to the 4f ground state to become lower. Hence, the increase in the probability for nonradiative energy transfer in 5d level causes a shift in emission peak toward longer wavelengths. This behavior was also observed in the case of $CaSi_2O_2N_2$:Eu^{2+} and $Ca_3Si_2O_4N_2$:Eu^{2+} [12,13], in which the emission energy from the 5d excited state is transferred to the lower levels, therefore resulting in the redshift of emission spectra. BMAS:Eu^{2+} exhibits a broad and strong PLE band peaking at around 254 nm, indicating that BMAS:Eu^{2+}can be used as a promising phosphor applied for fluorescent lamps.

In order to further understand the process of energy transfer, the fluorescence lifetimes τ_1 for Eu^{2+}(I) and τ_2 for Eu^{2+}(II) with different Eu^{2+} concentrations are measured and presented in Fig. 4. The fluorescence of Eu^{2+}(I) decays faster and tends to be a nonexponential function with increasing Eu^{2+} concentrations, reflecting the characteristics of energy transfer from donor Eu^{2+}(I) to acceptor Eu^{2+}(II) [14]. It can be seen that the lifetime of Eu^{2+}(II) is almost the same. Hence, we show the nonexistence of Eu^{2+}(II) concentration quenching within the range of Eu^{2+} concentrations of interest in this work.

Based on energy transfer, the dependences of the emission intensity ratios of Eu^{2+}(II) to Eu^{2+}(I) on Eu^{2+} concentration can be calculated by the measured fluorescence lifetimes of $Eu^{2+}(\tau_1)$ and $Eu^{2+}(\tau_2)$. Under steady excitation, the absorbing population of Eu^{2+}(I) is equal to the radiative population of the level. As for Eu^{2+}(II), the radiative population of the level is equal to the sum of the absorbing population and the population transfer from Eu^{2+}(I). So the rate equations describing the energy transfer from Eu^{2+}(I) to Eu^{2+}(II) can be written as follows:

$$f_1 = n_1/\tau_1 \tag{1}$$

$$f_2 + Wn_1 = n_2/\tau_2 \tag{2}$$

where f_1 and f_2 are the absorbing populations of Eu^{2+}(I) and Eu^{2+}(II), and n_1 and n_2 are the populations of Eu^{2+}(I) and Eu^{2+}(II) ions, respectively. The energy transfer rates W can be obtained by $W = 1/\tau_1\text{-}1/\tau_0$, since the fluorescence intensity of a specific level is proportional to the product of the population and the radiative rate of the level, using Eqs. (1) and (2), the dependences of the intensity ratio of the blue–ultraviolet emissions on Eu^{2+} concentrations can be written as

$$\frac{I_B}{I_U} \propto \frac{n_2\gamma_2}{n_1\gamma_1} = \frac{\gamma_2}{\gamma_1}\left(\frac{\tau_2 f_2}{\tau_1 f_1} + \tau_2 W\right) = \frac{\gamma_2}{\gamma_1}\left(\frac{\tau_2}{\tau_1}\left(\frac{f_2}{f_1} + 1\right) - \frac{\tau_2}{\tau_0}\right) \tag{3}$$

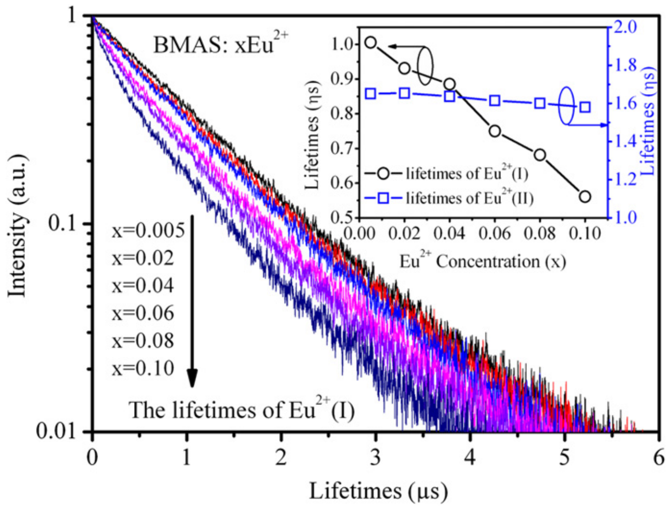

Fig. 4. Fluorescence decay curves of Eu^{2+}(I) with different Eu^{2+} concentrations. Inset: the calculated average lifetimes of Eu^{2+}(I) and Eu^{2+}(II).

where γ_1 and γ_1 are radiative rates of Eu^{2+}(I) and Eu^{2+}(II), respectively, which are independent of Eu^{2+} concentrations. τ_2 has been presented in the Fig. 4 inset. In Eq. (3), the γ_2/γ_1 and f_2/f_1 can be considered to be constants. Fig. 5 shows the intensity ratios I_B/I_U vs $1/\tau_1$ at various Eu^{2+} concentrations. It can be seen that the I_B/I_U goes linearly with $1/\tau_1$ when Eu^{2+} content is lower than 0.1, demonstrating that the energy transfer between Eu^{2+}(I) and Eu^{2+}(II) plays the main role on the I_B/I_U. The dots at $x = 0.04$ and 0.1 that deviate from straightness might be attributed to large variation of f_2/f_1 at these positions. In other words, when Eu^{2+} concentration is 0.04 mol, the distribution of Eu^{2+} at different sites may change significantly, leading to the change of f_2/f_1; when Eu^{2+} concentration is 0.1 mol, the saturated absorption population of Eu^{2+}(II) to Eu^{2+}(I) may vary remarkably at high Eu^{2+} concentrations, resulting in the variation of f_2/f_1.

Fig. 6 shows PL spectra of white light emitting BMAS:0.08Eu^{2+}, 0.08Tb^{3+}, and 0.16Mn^{2+} phosphor upon 254 nm excitation. The present phosphor shows four emission bands, ultraviolet band of 376 nm, blue band of 450 nm, green band of 542 nm and red band of 610 nm. Although a significant part of the energy at 376 nm

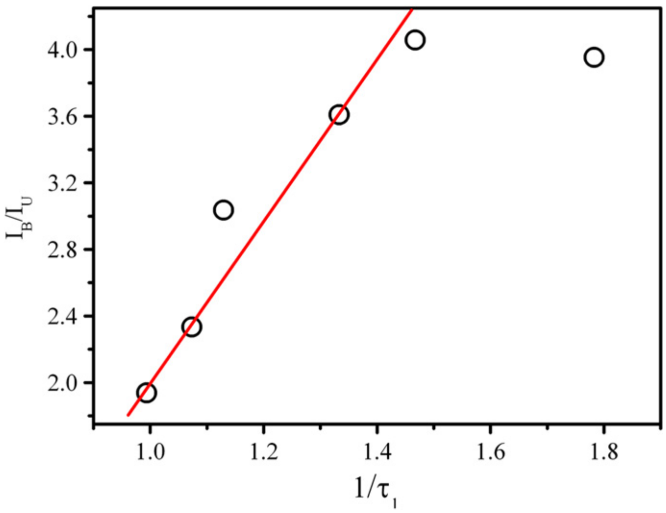

Fig. 5. Intensity ratios I_B/I_U vs $1/\tau_1$ at various Eu^{2+} concentrations.

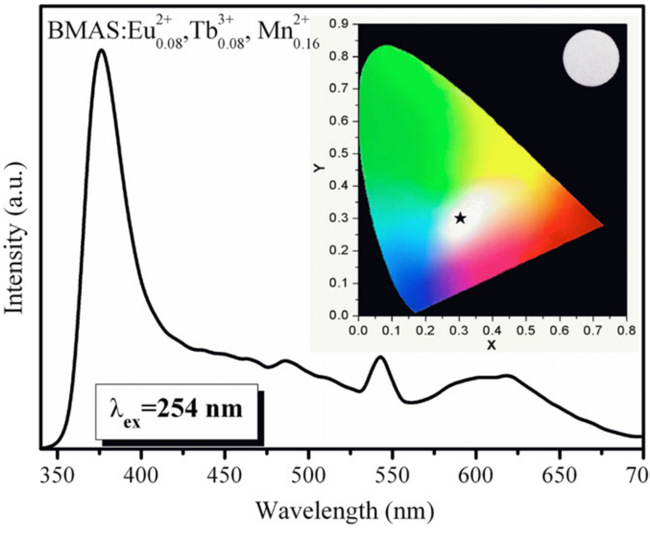

Fig. 6. PL spectra of white light emitting BMAS:0.08 Eu^{2+}, 0.08Tb^{3+}, and 0.16Mn^{2+} phosphor upon 254 nm excitation. Inset: the corresponding CIE color coordinates and photographs of this phosphor.

would lead to low quantum efficiency, the full-color emitting BMAS:Eu^{2+}, Tb^{3+}, and Mn^{2+} phosphors may be applied as potential phosphors for FLs. The emitting color point of a white light sample is illustrated in the CIE chromaticity diagram, as shown in the Fig. 6 inset. The corresponding CIE color coordinates of the phosphor are (0.29, 0.29). By using the optimized Eu^{2+} content at $x=0.08$, white light emitting BMAS:0.08 Eu^{2+}, 0.08Tb^{3+}, and 0.16Mn^{2+} phosphor can be generated upon 254 nm excitation. Our results indicate that BMAS:Eu^{2+}, Tb^{3+}, and Mn^{2+} are great potential candidates for using single phosphor converted white light source for recent FLs.

4. Conclusion

In conclusion, $BaMg_2Al_6Si_9O_{30}$:Eu^{2+} phosphors are synthesized by the solid-state reaction method and the energy transfer among Eu^{2+} ions is investigated. The energy transfer leads to the following results: (1) with increasing Eu^{2+} doping content, the blue emission bands shift gradually to longer wavelength and the PL intensity ratio of blue (I_B) to ultraviolet (I_U) emission increases; (2) the ratio of blue emission to ultraviolet emission by the experiment is analyzed by theoretical calculation based on energy transfer and lifetime measurements. By using the optimized Eu^{2+} content, the white light emitting BMAS:0.08Eu^{2+}, 0.08Tb^{3+}, and 0.16Mn^{2+} phosphor can be realized upon 254 nm excitation. The present letter indicates that our samples can be promising candidate phosphors for FLs.

Acknowledgments

This work is financially supported by the National Nature Science Foundation of China (10834006, 10904141, 10904140, 51172226), the MOST of china (2010AA03A404) and the Scientific Project of Jilin province (20090134, 20090524) and CAS Innovation Program.

References

[1] Y. Shimomura, N. Kijima, J. Electrochem. Soc. 151 (8) (2004) H192–H197.
[2] Y. Shimomura, N. Kijima, J. Electrochem. Soc. 151 (4) (2004) H86–H92.
[3] W. van Schaik, S. Lizzo, W. Smit, G. Blass, J. Electrochem. Soc. 140 (1) (1993) 216–222.
[4] C.H. Huang, T.W. Kuo, T.M. Chen, Opt. Express 19 (2011) A1–A6.
[5] C.H. Huang, T.W. Kuo, T.M. Chen, ACS Appl. Mater. Interfaces **2** (5) (2010) 1395–1399.
[6] T.W. Kuo, T.M. Chen, J. Electrochem. Soc. 157 (6) (2010) J216–J220.
[7] T.W. Kuo, C.H. Huang, T.M. Chen, Appl. Opt. 49 (2010) 4202–4206.
[8] T.W. Kuo, T.M. Chen, Opt. Mater. 32 (2010) 882–885.
[9] W. Lü, Z.D. Hao, X. Zhang, Y.S. Luo, X.J. Wang, J.H. Zhang, Inorg. Chem. 50 (2011) 7846–7851.
[10] W. Wolfgang, T. Armbruster, C. Lengauer, Eur. J. Mineral. 7 (1995) 277–286.
[11] W. Lü, X. Zhang, Y. Wang, Z.D. Hao, Y.F. Liu, Y.S. Luo, X.J. Wang, J.H. Zhang, J. Alloys Compd. 513 (2012) 430–435.
[12] Y.C. Chiu, C.H. Huang, T.J. Lee, W.R. Liu, Y.T. Yeh, S.M. Jang, R.S. Liu, Opt. Express 19 (2011) A331–A339.
[13] X.F. Song, R.L. Fu, S. Agathopoulos, H. He, X.R. Zhao, S.D. Zhang, J. Appl. Phys. 106 (2009) 033103–033105.
[14] M.M. Broer, D.L. Huber, W.M. Yen, W.K. Zwicker, Phys. Rev. Lett. 49 (1982) 394–398.